Computational exploration of natural inhibitors against toxin-associated proteins in *Naegleria fowleri* Karachi strain

Rabia Faizan [a], Muhammad Naveed [b], Inmaculada Bellido Estevez [a], Nimra Hanif [b], Arooj Arshad [b], Tariq Aziz [c], Abdulhakeem S. Alamri [d], Walaa F. Alsanie [d], Majid Alhomrani [d]

https://doi.org/10.1016/j.prp.2025.156184

Abstract

Naegleria fowleri, a thermophilic, free-living amoeba, is the causative agent of Primary Amoebic Meningoencephalitis (PAM), a rare but nearly always fatal brain infection. The rising number of PAM cases in Karachi, Pakistan, particularly linked to a unique local strain, underscores the urgent need for effective therapeutic interventions. In this study, a computational approach was employed to identify potential natural inhibitors targeting toxin-producing proteins from the *N. fowleri* Karachi strain. Eight exons encoding toxin proteins were retrieved from the Soft Berry Fgenesh 2.6 database, annotated using Gene Ontology tools, and subjected to physicochemical characterization. Hypothetical protein 4 was prioritized for molecular docking in the NF001 Karachi strain of *Naegleria fowleri* because it was identified through comparative mapping with previously known strains. Its function was predicted based on sequence alignment, suggesting that it may serve as a promising target for drug docking studies. Protein structures were predicted via AlphaFold2 and validated using MolProbity and Ramachandran plot analysis. Virtual screening of phytochemicals was conducted using PyRx, identifying himbacine as the most promising ligand with a binding affinity of –8.7 kcal/mol against hypothetical protein 4. Binding interactions were further confirmed using CB-Dock2, which revealed key binding residues involved in hydrogen bonding and hydrophobic interactions. ADMET profiling indicated that himbacine possesses favorable pharmacokinetics, non-toxicity, and high gastrointestinal absorption. Density Functional Theory (DFT) analysis showed a small HOMO-LUMO energy gap, indicating high reactivity and binding potential. Molecular dynamics simulations confirmed the structural stability of the protein-ligand complex over time. These findings suggest that himbacine, a plant-derived compound, holds promise as a safe and effective inhibitor against *N. fowleri* infections. However, further in vitro and in vivo studies are essential to validate its therapeutic potential.

Keywords

Naegleria fowleri, Brain-eating amoeba, Computational drug design, Himbacine
ADMET analysis, Molecular docking

1. Introduction

Naegleria fowleri is a free-living thermophilic amoeba and globally present in soil and warm fresh water. Among all *Naegleria genus* only *Naegleria fowleri* species cause disease in human commonly known as primary amoebic meningoencephalitis (PAM) and mostly affects the children and young adults [1]. The life cycle of *Naegleria fowleri* is categorized into three phase. Phase 1 contains cyst formation while in 2 and 3 phases amoeba convert into a trophozoite which mostly involved in causing infection and a flagellate, respectively [2]. The shape of trophozoite is single-nucleated granular having a diameter of 10–30 μm and replicate through binary fission. While in extreme environment such as nutrients deficiency trophozoite takes the form of flagellates which are 10–16 μm in length. Trophozoite can be diagnosed through cerebrospinal fluid and tissue, but flagellates are rarely deducted in the cerebrospinal fluid (CSF). Whereas, the cyst form of amoeba is not frequently discovered in brain tissue [3]. Although the host possesses numerous physical and immunological barriers that typically prevent microbial invasion, certain protozoa like *Naegleria fowleri* have evolved mechanisms to overcome these defenses, resulting in severe disease and often fatal outcomes. Therefore, elucidating the molecular factors and pathogenic mechanisms involved in primary amoebic meningoencephalitis (PAM) is essential for the

development of effective therapeutic strategies [4]. *Naegleria fowleri* infections begin with trophozoite attachment to the nasal mucosa after pathogen-containing water enters the cavity. The pathogen then travels to the olfactory bulbs in the central nervous system (CNS) via the olfactory nerve and the cribriform plate. This results in a robust immunological response by activating the innate immune system. The first PAM case was reported in Karachi in 2008. In 2019, the number reached 146, surpassing the total number of cases documented in the United States from 1968 to 2019. Furthermore, in Karachi, *Naegleria fowleri* is primarily transmitted through water, leading to PAM, making it a waterborne disease. In United State, most of the PAM cases reported involved children less than 14 years old, while in Pakistan infected people were young having age 26–45 years. There are no established treatment methods for *N. fowleri* due to the rarity of PAM in humans worldwide [5].

Flavonoids, alkaloids, and terpenes are examples of natural substances with antimicrobial action that are crucial to the immune system's defense mechanism. Natural products play an important role in the discovery of bioactive chemicals [6]. These substances are less likely to cause side effects than conventional treatments, less expensive, and safer than certain synthetic drugs [7]. The development of natural product system show robust effects but more clinical research is needed to better understand how to use natural products with modern pharmaceuticals and enhance delivery systems. In order to treat PAM, many natural inhibitors have been screened out to restrict its replication in host cell. In this study we will target eight exons coding toxin protein present in the genome of *Naegleria fowleri* Karachi strain [8]. There are few published studies on bioinformatics- assisted drug design on pharmacological compounds for treating the unique strain of *Naegleria fowleri* found in Karachi, which brings gap to our knowledge. Computational tools were employed to design a drug candidate that showed promising effects against infections caused by the *Naegleria fowleri* Karachi strain.

The pathogenicity of *Naegleria fowleri* has been described in numerous research studies. Genomic analyses have identified a variety of genes associated with its virulence and other critical functions. Among the key pathogenic factors are several proteins that enable the organism to damage brain cells. A unique structure “food-cup,” which contains *Naegleria fowleri* antigen-1 (Nfa1). This antigen is highly expressed in the pseudopodia—cellular extensions involved in the amoeba’s movement and plays a crucial role in phagocytosis by facilitating attachment to host cells.

Naegleria fowleri secretes a range of proteolytic enzymes that assist in breaking down the host cell, aiding the engulfment process. As such, pseudopodia are thought to be central to the contact-dependent mechanisms underlying *N. fowleri* pathogenicity. Detailed knowledge of the structure of proteolytic enzymes and their ligand-binding properties is essential for identifying potential targets and developing effective therapeutic drugs [9].

There are no published studies proposing any drug compounds for use against this novel strain of *Naegleria fowleri* from Karachi. Therefore, the purpose of the present in-silico study is to analyze the known protein products of 5 of the 15 unique genes, identified in the Karachi strain by determining their structure, active sites, and docking them with selected ligand compounds (potential drug candidates) to treat the novel Karachi strain. The sequencing yielded 15 unique genes, 6 of them with known protein products, not found in the genome of any other reported *Naegleria fowleri* strains worldwide [10].

The present study integrates these computational methods to identify natural inhibitors targeting toxin-producing proteins of the *Naegleria fowleri* Karachi strain. Recent advances in computational biology have significantly accelerated the drug discovery process by enabling virtual screening, molecular docking, and predictive modeling of pharmacokinetic and toxicological properties. These tools enhance the efficiency and accuracy of identifying bioactive compounds while substantially reducing experimental costs and time. In the context of neglected pathogens like *Naegleria fowleri*, where conventional drug discovery is limited due to low incidence and poor commercial interest, in silico approaches provide a powerful and economical alternative. This methodology not only streamlines the identification of potential therapeutic

candidates but also offers insights into their pharmacological profiles, thereby aligning with the study's goal of proposing novel, plant-based treatment strategies against PAM.

2. Materials and methods

2.1. Retrieval of toxin proteins

Naegleria fowleri Karachi-NF001 strain (accession OD956727.1) was retrieved through NCBI's protein database (https://www.ncbi.nlm.nih.gov/) [11] and eight toxin proteins were using SoftBerry Fgenesh 2.6. Fgenesh+ aligned homologous proteins onto genomic sequences and detected exon boundaries through integrated protein database alignments and HMM-based gene modeling. Functional annotation used UniProt-GO (https://geneontology.org/docs/go-enrichment-analysis/) databases [12], integrating electronic predictions with manual curation to categorize proteins into families.

2.2. Physiochemical analysis

Physiochemical characteristics of toxin proteins were analyzed through the use of the ExPASy Protparam (https://web.expasy.org/protparam/) Protein sequences were entered determining molecular weight, amino acid composition, theoretical pI, instability index, aliphatic index, and GRAVY score. The parameters gave indications regarding protein stability, hydrophobicity, and charge distribution from computational prediction from primary sequences [13].

2.3. Structure prediction and validation

Tertiary structures were predicted using AlphaFold 3 (https://alphafold.ebi.ac.uk/) [14] and structure quality was checked using MolProbity (http://molprobity.biochem.duke.edu/) [15] by examining Ramachandran plots. The Ramachandran plot measured amino acid residues in favored and allowed regions and also predict how many residues are outliers which are not in favored region, with implications for structural quality and accuracy.

2.4. Retrieval of natural inhibitors

Five natural inhibitors were retrieved from the PubChem database (https://pubchem.ncbi.nlm.nih.gov/),which provided their tertiary structures, molecular weights, and compound IDs. The natural compounds selected in this study himbacine (alkaloid), berberine (alkaloid), quercetin (flavonoid), artemisinin (terpene), and eugenol (phenolic compound)—were chosen based on their previously reported pharmacological properties, particularly antibacterial, anti-inflammatory, and neuroprotective effects. Their structural diversity offered a broad range of interaction potentials with the target proteins. Moreover, some of these compounds have shown promising results in earlier computational or in vitro studies against protozoal pathogens. These bioactivities are especially relevant in addressing Naegleria fowleri, a pathogen that triggers severe inflammation and damages brain tissues [16] [17].

2.5. Molecular docking analysis

Screening of natural inhibitors was performed virtually using PyRx [18], which incorporates AutoDock Vina for docking simulations. Protein structures were prepared by removing water molecules and adding polar hydrogens, while ligands retrieved from PubChem were converted and energy-minimized using Open Babel with the Universal Force Field (UFF). Both proteins and ligands were saved in PDBQT format. Docking was performed with default Vina settings, and the grid box was automatically set to cover the predicted active site. Binding affinities were calculated based on Vina's scoring function, and top-ranked poses were selected for further analysis. Firslty, receptor (protein) was converted into pdbqt file format and then energies of all selected ligands were minimized to make pdbqt file for screening. The proteins and ligands were converted into compatible formats, and the ligand energies were minimized. CB-Dock2 (https://cadd.labshare.cn/cb-dock2/index.php) a cavity detection tool was then utilized for validation of molecular docking. [19] to validate ligand-protein interactions. This tool works by

automatically detecting potential binding sites (cavities) on the protein surface and then docking the ligand into those regions. The protein and ligand structures were uploaded in PDB format, after which the tool generated predicted cavities based on shape complementarity and physicochemical properties. It then performed docking simulations using AutoDock Vina, providing the binding affinity scores and visualizing the top-ranked binding poses. Discovery Studio was employed for predicting 2D and 3D interaction.

2.6. ADMT analysis

The ADMET (Absorption, Distribution, Metabolism, Excretion, and Toxicity) properties of the top-performing compound, himbacine, were predicted using two online platforms: AdmetSAR 2.0 (http://lmmd.ecust.edu.cn/admetsar2) [20], and SwissADME (http://www.swissadme.ch/) [21]. The SMILES notation of himbacine, obtained from the PubChem database, was used as input for both tools. AdmetSAR 2.0 was used to assess parameters such as blood-brain barrier permeability, human intestinal absorption, P-glycoprotein interactions, and CYP450 enzyme inhibition or substrate potential. SwissADME was used to evaluate drug-likeness based on Lipinski's rule of five, molar refractivity, topological polar surface area, and gastrointestinal absorption. All tools were accessed online using their default models and prediction settings to ensure standardization and reproducibility of results.

2.7. Toxicity analysis

The ligand's in silico toxicity was assessed using ProTox-II, a web-based virtual toxicity prediction platform (https://tox-new.charite.de/protox_II). The compound's SMILES notation was submitted to the server for prediction of several toxicity endpoints, including toxicity class and probable toxicological effects such as hepatotoxicity, carcinogenicity, immunotoxicity, mutagenicity, and cytotoxicity [22].

2.8. Density functional theory analysis

In order to assess the bioreactivity of himbacine as a drug candidate, DFT calculations were carried out using GaussView (https://gaussian.com/gaussview6/) for molecular drawing and Gaussian for DFT analysis. The 3D structure of Himbacine was either downloaded from a file in GaussView. Then, it was followed by geometry optimization. Subsequently, the optimized structure was used as an input for DFT analysis with B3LYP (Becke, 3-parameter, Lee-Yang-Parr) hybrid functional employing 6–31 G basis set. The calculation was performed in the ground state with singlet spin multiplicity (S = 0) and neutral charge. The band gap energy (E_gap) which offers information about the molecules strength of chemical bonds and reactivity, was calculated alongside Highest occupied molecular orbital energy (eHOMO) and Lowest unoccupied molecular energy (eLUMO). Together with GaussView, the region of dense electron concentration that can be responsible for binding of a molecule were visualized [23].

2.9. Molecular dynamic simulation

Molecular dynamic simulation was performed by using Desmond (https://www.schrodinger.com/desmond) [24] tool at 100 ns. During MD simulation analysis, protein-himbacine complex, root mean square deviation (RMSD), root mean square fluctuation (RMSF), and secondary structure elements (SSE) timeline were carried out to evaluate the dynamics and stability of ligand and protein complex. The Root Mean Square Deviation (RMSD) is used to measure the average change in displacement of a selection of atoms for a particular frame with respect to a reference frame. The Root Mean Square Fluctuation (RMSF) determined for characterizing the local changes along the protein chain. Further Protein interactions with the ligand can be monitored throughout the simulation. Protein-ligand interactions are categorized into four types: Hydrogen Bonds, Hydrophobic, Ionic and Water Bridges.

3. Results

3.1. Retrieval of toxin proteins and functional analysis

Toxin proteins of *Naegleria fowleri* Karachi_NF001 strain were retrieved from SOFTBERRY FGENESH 2.6 data bases with accession number OD956727.1. Functional annotation was performed through Uniprot and Gene ontology database which validate the protein families and their functions. Table 1 depicted that Exons (E1, E2, E3, and E5) coding proteins belong to RNase H type-1 domain-containing protein, Ion trans domain-containing protein, and MIR domain-containing protein and SURF1-like protein respectively and remaining proteins are hypothetical proteins (Table 1).

Table 1. Functional annotation and protein family prediction of exons.

Exons	Protein family	Function
1	RNase H type−1 domain-containing protein	nucleic acid binding
2	Ion_trans domain-containing protein	monoatomic ion channel activity
3	MIR domain-containing protein	calcium ion transmembrane transport
4	Hypothetical protein	
5	SURF1-like protein	mitochondrial inner membrane
6	Hypothetical protein(DUF4252 domain-containing protein)	
7	Hypothetical (Polymerase nucleotidyl transferase domain-containing protein)	Nucleotidyltransferase
8	Hypothetical protein (DNA double-strand break repair and VJ recombination XRCC4, N-terminal 1 hit)	DNA repair

3.2. Physiochemical analysis

Physiochemical properties of all toxin proteins was predicted by Expasy Protparam tool. Table 2 has been showing the total number of amino acid residues, molecular weight, total number of negatively and positively charge residue, theoretical pI that showed the protein nature, instability index for determining either protein is stable or unstable if its value is less than 40 then protein is stable and if the value is above 40 then protein would be unstable, aliphatic index, and Grand average of hydropathicity (GRAVY) indicting protein hydrophilic or hydrophobic nature.

Table 2. Physiochemical properties of proteins.

Proteins	Number of amino acid residues	Molecular weight	Negatively charge residues	Positively charge residues	Theoretical pI	Instability index	aliphatic index	GRAVY
Exon1	276	31168.14	25	34	9.15	23.32	99.17	−0.207
Exon2	377	43943.24	32	41	9.22	31.67	98.73	0.189
Exon3	2210	254475.05	270	289	8.69	45.76	89.14	−0.435
Exon4	223	25145.45	29	25	5.65	48.88	86.82	−0.418
Exon5	173	19975.12	15	23	9.40	48.43	81.73	−0.280

Proteins	Number of amino acid residues	Molecular weight	Negatively charge residues	Positively charge residues	Theoretical pI	Instability index	aliphatic index	GRAVY
Exon6	191	21025.76	17	22	9.41	43.03	84.71	−0.303
Exon7	350	40786.65	49	49	7.26	54.09	80.74	−0.613
Exon8	460	52489.50	60	54	6.01	64.03	74.61	−0.831

3.3. Structure prediction and validation

Protein tertiary structure was predicted by Alpha fold 3 (Fig. 1) then further validate the structure quality by PROCHECK tool providing results in Ramachandran plot (Fig. 2). By using Ramachandran plot, it was depicted that in protein 1, 90.4 % of all residues were in favored (98 %) regions, 98.4 % of all residues were in allowed regions, and 6 outliers residues. In protein 2, 93.3 % of all residues were in favored (98 %) regions, 98.3 % of all residues were in allowed (>99.8 %) regions, and there were 10 outliers residues. In protein 3, 98.2 % of all residues were in favored (98 %) regions, 99.9 % of all residues were in allowed (>99.8 %) regions, and no outliers residue. In protein 4, 89.9 % of all residues were in favored (98 %) regions, 96.6 % (345/357) of all residues were in allowed (>99.8 %) regions and 12 outliers residues. In protein 5, 90.3 % of all residues were in favored (98 %) regions, 96.8 % of all residues were in allowed (>99.8 %) regions, and 13 outliers residues. In protein 6, 82.0 % of all residues were in favored (98 %) regions, 93.1 % of all residues were in allowed (>99.8 %) regions and 13 outliers residues. In protein 7, 97.9 % of all residues were in favored (98 %) regions, 99.8 % of all residues were in allowed (>99.8 %) regions and only 3 outliers residue. In protein 8, 97.4 % of all residues were in favored (98 %) region, 99.6 % of all residues were in allowed (>99.8 %) regions, and 2 outliers residues.

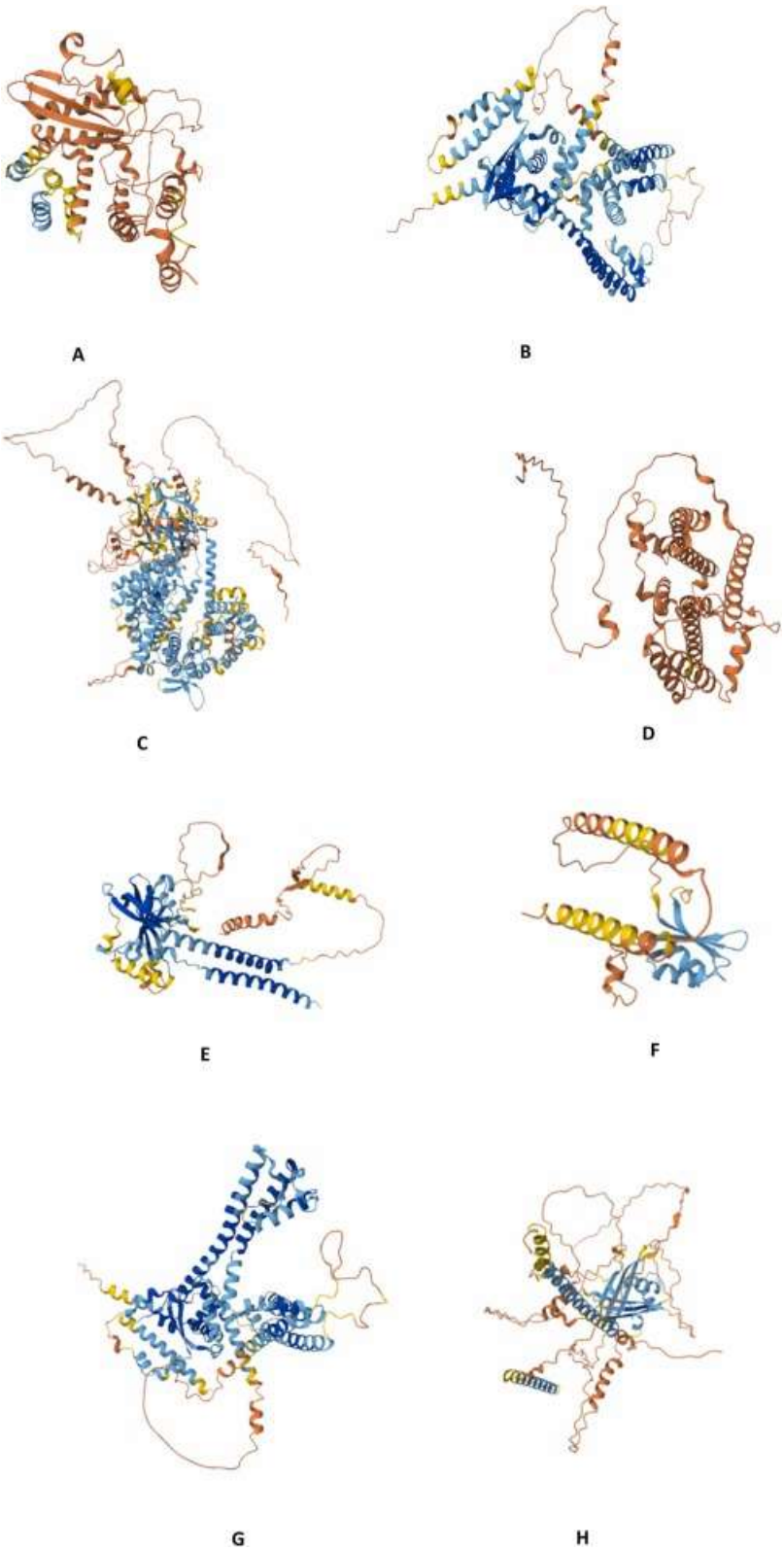

Fig. 1. Tertiary structure of toxin proteins predicted by Alphafold 3. **A**: Tertiary structure of protein 1. **B**: Tertiary structure of protein 2. **C**: Tertiary structure of protein 3. **D**: Tertiary structure of protein 4. **E**: Tertiary structure of protein 5. **F**: Tertiary structure of protein 6. **G**: Tertiary structure of protein 7. **H**: Tertiary structure of protein 8.

(A)

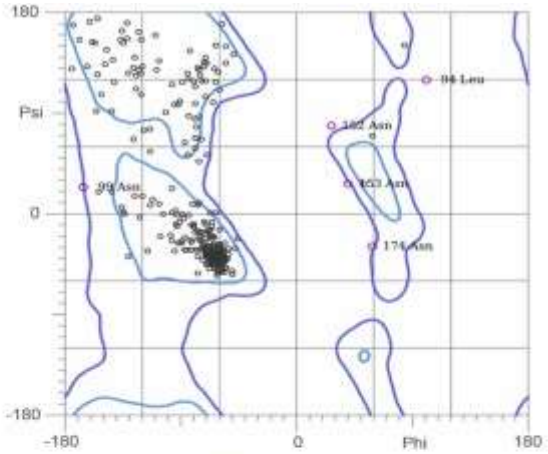
180
Psi
0
-180
-180
0
Phi
180
94 Leu
182 Asn
99 Asn
153 Asn
174 Asn

(B)

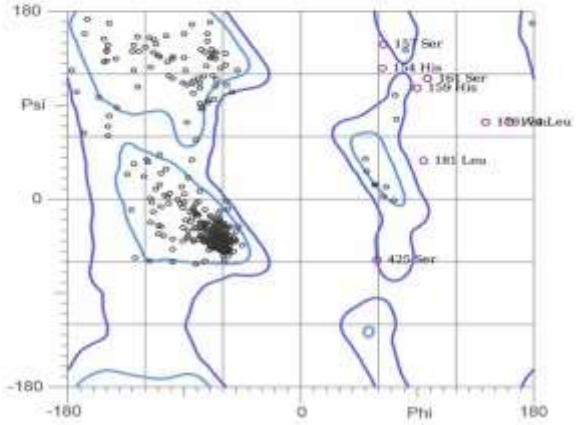
180
Psi
0
-180
-180
0
Phi
180
137 Ser
154 His
181 Leu
425 Ser

(C)

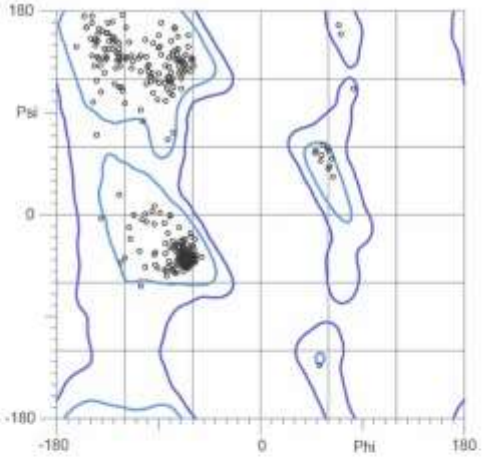
180
Psi
0
-180
-180
0
Phi
180

(D)

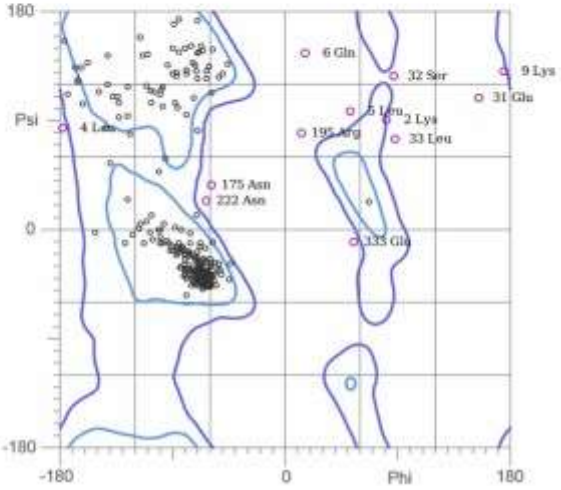
180
Psi
0
-180
-180
0
Phi
180
6 Gln
32 Ser
9 Lys
31 Glu
5 Leu
2 Lys
4 Leu
195 Arg
33 Leu
175 Asn
222 Asn
135 Glu

(E)

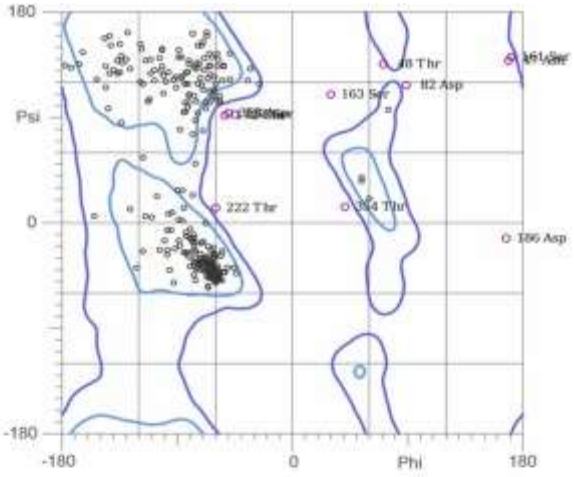
180
Psi
0
-180
-180
0
Phi
180
8 Thr
163 Ser
182 Asp
222 Thr
186 Asp

(F)

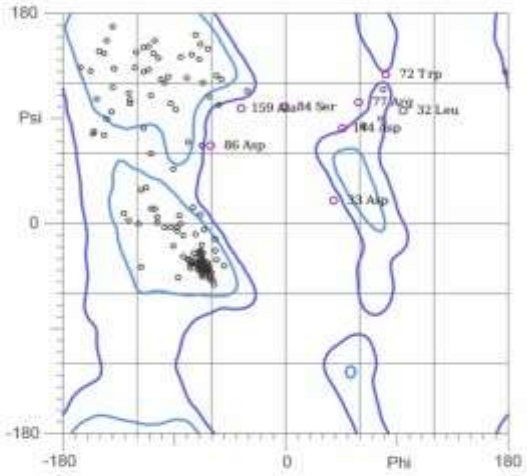
180
Psi
0
-180
-180
0
Phi
180
72 Trp
159 Ala
84 Ser
77 Asp
32 Leu
86 Asp
33 Asp

(G)

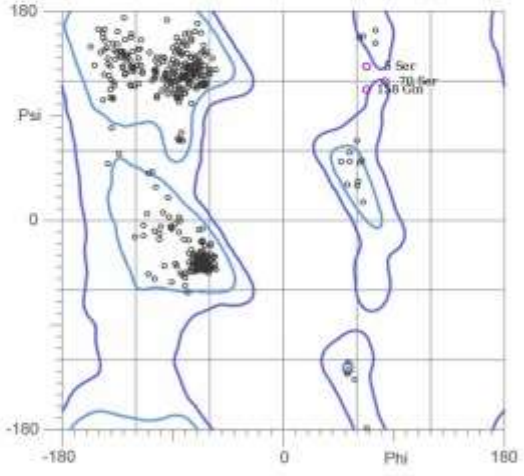
180
Psi
0
-180
-180
0
Phi
180
5 Ser
70 Ser
156 Gln

(H)

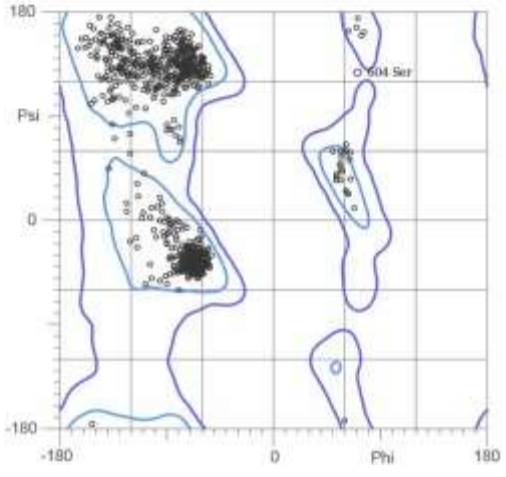
180
Psi
0
-180
-180
0
Phi
180
604 Ser

Fig. 2. Ramachandran plot analysis of the predicted 3D structures of Naegleria fowleri toxin proteins generated using MolProbity. **A**: Ramachandran Plot validating the 3D structure of protein 1. **B**: Ramachandran Plot validating the 3D structure of protein 2. **C**: Ramachandran Plot validating the 3D structure of protein 3. **D**: Ramachandran Plot validating the 3D structure of protein 4. **E**: Ramachandran Plot validating the 3D structure of protein 5. **F**: Ramachandran Plot validating the 3D structure of protein 6. **G**: Ramachandran Plot validating the 3D structure of protein 7. **H**: Ramachandran Plot validating the 3D structure of protein 8.

3.4. Retrieval of natural inhibitors

Five natural inhibitors were taken from PubChem database. Phytochemicals 2D and 3D tertiary structures, molecular weight, and compounds ID given by PubChem database have been listed in Table 3.

Table 3. List of five natural inhibitors against *Naegleria fowleri* toxin proteins, including 2D/3D structures, molecular weights, and PubChem CIDs.

Natural inhibitors	Compounds ID	Tertiary structure	Molecular weight	Secondary structure
Himbacine	CID:6436265		345.5 g/mol	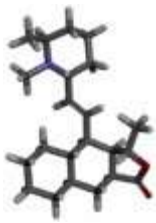
Berberine	CID: 2353	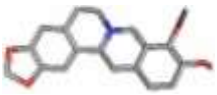	336.4 g/mol	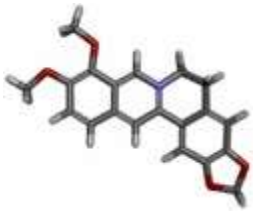
Quercetin	CID: 5280343		302.23 g/mol	
Artemisinin	CID: 68827		282.33 g/mol	
Eugenol	CID: 3314		164.2 g/mol	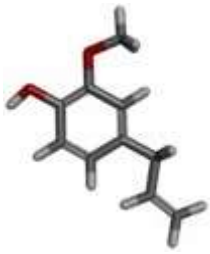

3.5. Molecular docking analysis

Virtual screening of all natural inhibitors was performed via PyRx and CB-dock2 tool was employed to further validate the molecular docking between ligand and proteins. Docking results predicted that hembacin showed highest binding energy of −8.7 kcal/mol with exon 4 protein among all other proteins and ligands. Table 4 has been showing the binding affinity of all protein with ligands. Fig. 3 has been showing the ligand and dock complex of all proteins with amino acid residues of proteins which involved in interaction with ligands. Protein residues interact with ligand through many bonds interactions including hydrogen bonds, van der Waals, alkyl and Pi-Alkyl, and Pi-Pi stacked ionic interactions visualized by Discovery studio as shown in Fig. 3. Docking analysis showed that himbacine interacts with TYR199, ILE228, VAL341, LEU206, LYS342, VAL203, VAL210, ASP338, MET103, PHE137, and GLY346 of protein1, HIS94, HIS98, THR480, ILE507, VAL97, LEU513, PHE484, ILE479, PHE503, GLU504, and LYS490 of protein 2, GLY102, TYR371, LYS399, TYR370, ALA398, ARG417, VAL402, ARG372, ALA401, and SER374 of protein 3, PHE72, TYR334, GLU69, ILE338, LEU294, HIS301, LEU297, and TYR298 of protein 4, THR280, PHE328, TYR329, VAL279, VAL359, ARG247, TYR199, ALA327, PRO357, LYS355, ASP353, and GLN352 of protein 5, VAL137, GLY114, HIS111, LEU115, ASN107, ALA110, ARG117, VAL135, LYS116, MET138, and ASP139, of protein 6, TRP436, ILE226, PHE432, ASN227, LEU461, LEU460, TYR477, ALA464, LEU231, VAL457, and ARG223 of protein 7, and PHE370, CYS374, ILE376, TYR418, ASN371, ARG415, THR410, ILE318, GLN314, and LEU414 of protein 8. Fig. 3 and 4 has been showing the dock complex and 2d structure of himbacine and toxin proteins.

Table 4. Binding affinities of ligands with toxin proteins of *Naegleria fowleri*.

Proteins	**Himbacine**	**Berberine**	**Quercetin**	**Artemisinin**	**Eugenol**
1	−7.5	−6.2	−6.5	−6.00	−5.1
2	−8.8	−6.1	−7.00	−5.9	−5.6
3	−8.6	−7.00	−6.9	−6.1	−5.5
4	−8.9	−7.4	−7.2	−7.3	−6.2
5	−7.8	−7	−6.00	−6.2	−5.1
6	−8	−7.1	−6.1	−6.2	−5.2
7	−7.6	−5.9	−5.8	−5.5	−5.00
8	−8.6	−6.00	−7.00	−5.7	6.00

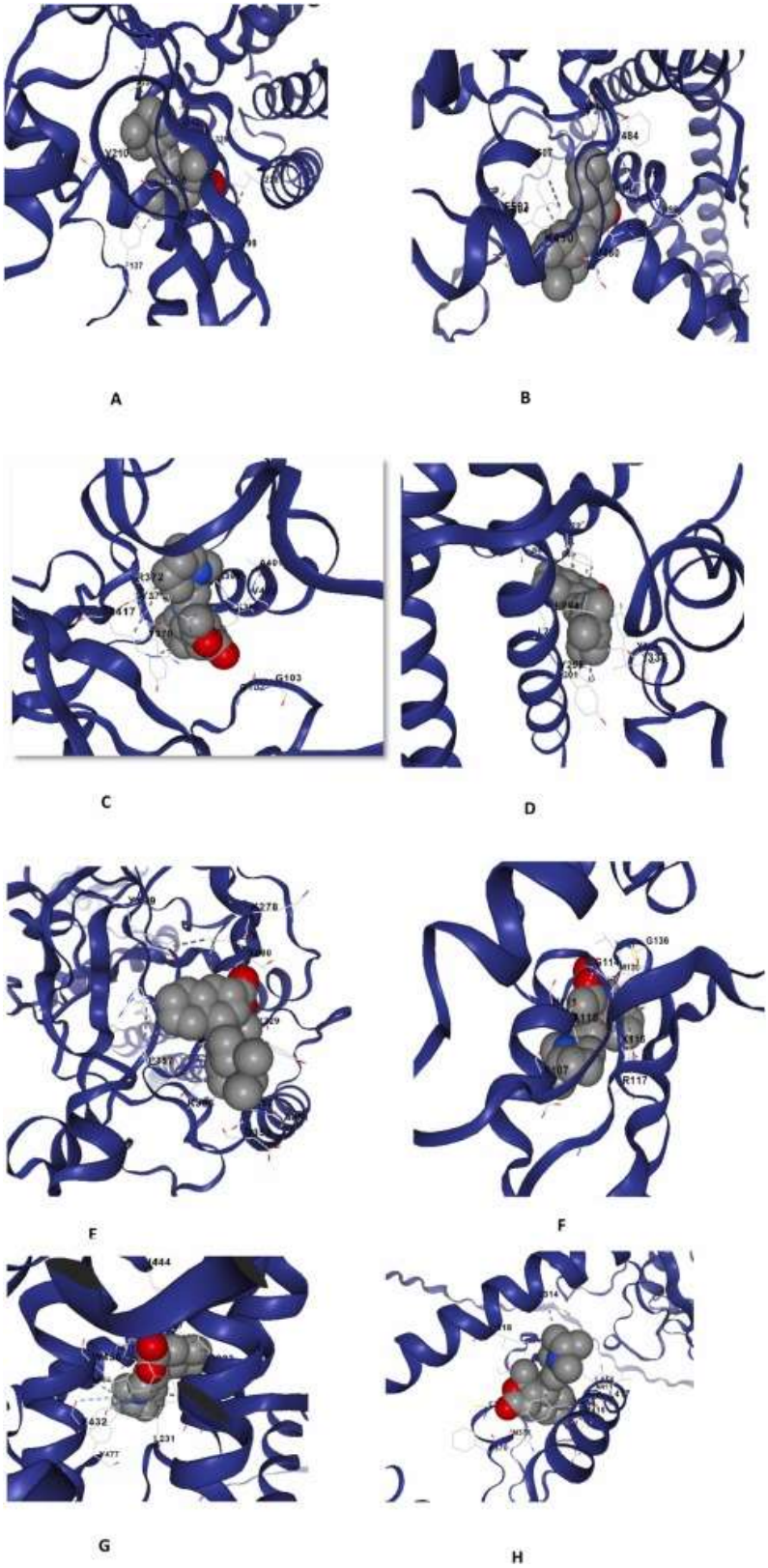

Fig. 3. Dock complex of himbacine with all toxin protein of *Naegleria fowler*i. **A**: Dock complex of himbacine and protein 1. **B**: Dock complex of himbacine and protein 2. **C**: Dock complex of himbacine and protein 3. **D**: Dock complex of himbacine and protein 4. **E**: Dock complex of himbacine and protein 5. **F**: Dock complex of himbacine and protein 6. **G**: Dock complex of himbacine and protein 7. **H**: Dock complex of himbacine and protein 8.

(A)

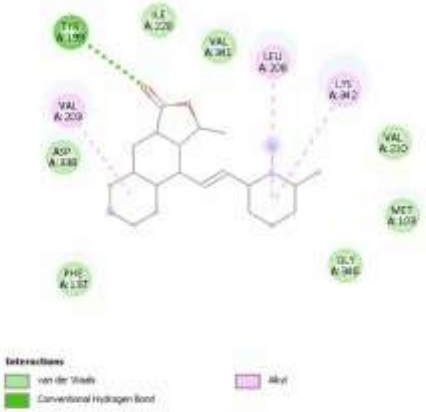
Interactions
van der Waals
Conventional Hydrogen Bond
Alkyl

(B)

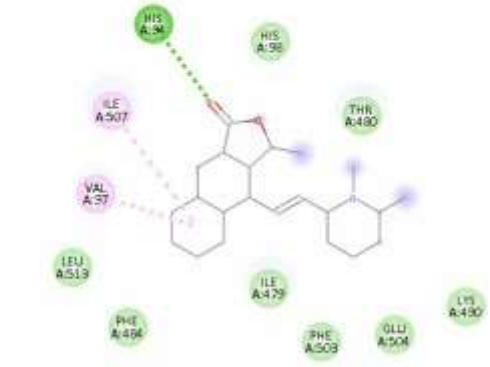
Interactions
van der Waals
Conventional Hydrogen Bond
Alkyl

(C)

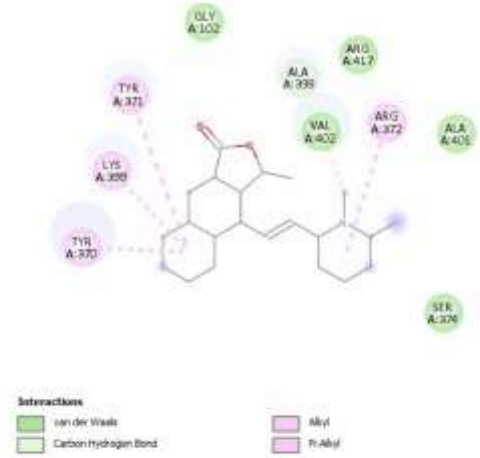
Interactions
van der Waals
Carbon Hydrogen Bond
Alkyl
Pi-Alkyl

(D)

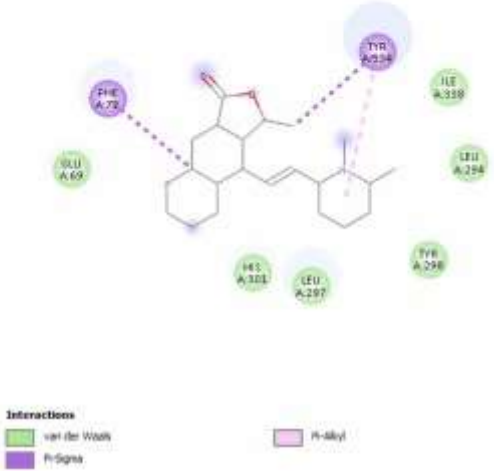
Interactions
van der Waals
Pi-Sigma
Pi-Alkyl

(E)

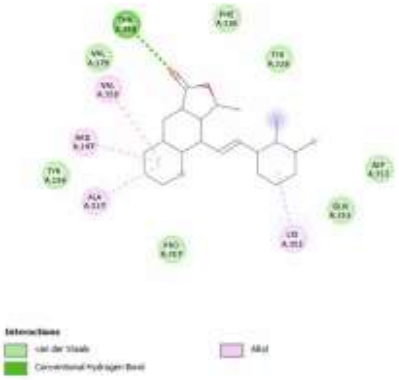
Interactions
van der Waals
Conventional Hydrogen Bond
Alkyl

(F)

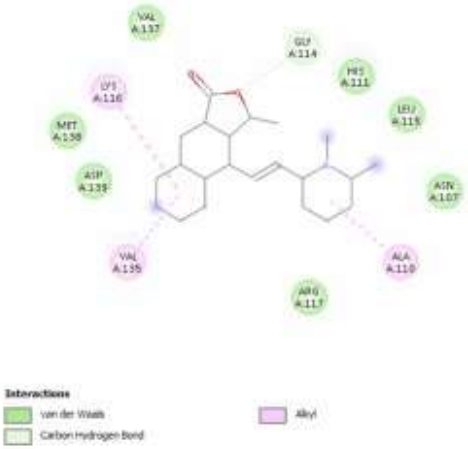
VAL A:137
GLY A:114
HIS A:111
LYS A:116
LEU A:115
MET A:138
ASP A:139
ASN A:107
VAL A:135
ALA A:110
ARG A:117
Interactions
van der Waals
Carbon Hydrogen Bond
Alkyl

(G)

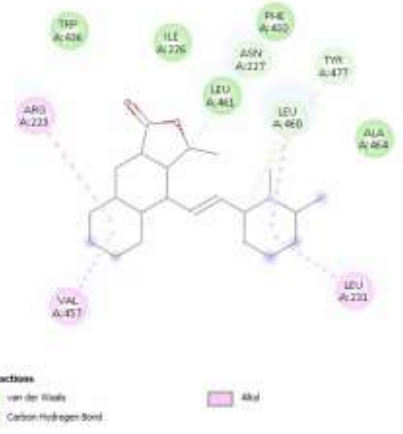
TRP A:426
ILE A:226
PHE A:402
ASN A:227
TYR A:477
LEU A:461
LEU A:460
ARG A:223
ALA A:464
LEU A:231
VAL A:457
Interactions
van der Waals
Carbon Hydrogen Bond
Alkyl

(H)

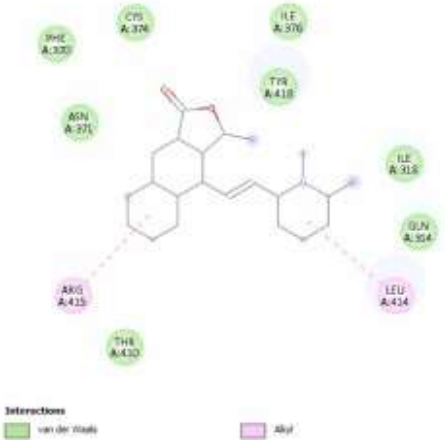
CYS A:374
ILE A:370
PHE A:330
TYR A:418
ASN A:371
ILE A:318
GLN A:314
ARG A:415
LEU A:414
THR A:430
Interactions
van der Waals
Alkyl

Fig. 4. 2D interactions of himbacine with all toxin proteins of *Naegleria flowri*. **A**: 2D interactions of himbacine with toxin protein 1. **B**: 2D interactions of himbacine with toxin protein 2. **C**: 2D interactions of himbacine with toxin protein 3. **D**: 2D interactions of himbacine with toxin protein 4. **E**: 2D interactions of himbacine with toxin protein 5. **F**: 2D interactions of himbacine with toxin protein 6. **G**: 2D interactions of himbacine with toxin protein 7. **H**: 2D interactions of himbacine with toxin protein 8.

3.6. ADMET analysis

AdmetSAR was employed to predict the ADMET (absorption, distribution, metabolism, excretion, and toxicity) characteristics of the natural inhibitor himbacine, which could be proven an effective therapeutic agent as a natural a natural inhibitor. Table 5 has been showing the ADMET analysis. According to Lipinski's rule of 5 predicted by SwissADME tool determining the topological molar surface area (29.54 Å2) and other different parameters as depicted in Table 6 and n-violations that indicating the total number of violations that is 0 in our drug candidate against *Naegleria fowleri*. Himbacine demonstrated high gastrointestinal absorption and favorable blood-brain barrier permeability, making it particularly suitable for targeting infections in the central nervous system such as Primary Amoebic Meningoencephalitis (PAM)

Table 5. ADMET profile of himbacine inhibitor.

Empty Cell	**ADMET parameters**	**Values**
	Blood-Brain Barrier	0.9783
Absorption	Human Intestinal Absorption	1.0000
	Caco−2 Permeability	0.7896
	P-glycoprotein Substrate	0.5714
	P-glycoprotein Inhibitor	0.6440
Excretion	Renal Organic Cation Transporter	0.5114
	Aqueous solubility	−2.8549
Distribution	Subcellular localization	0.3880
	CYP450 2C9 Substrate	0.8060
	CYP450 2D6 Substrate	0.5611
	CYP450 3A4 Substrate	0.7095
	CYP450 1A2 Inhibitor	0.5903
Metabolism	CYP450 2C9 Inhibitor	0.9143
	CYP450 2D6 Inhibitor	0.7224
	CYP450 2C19 Inhibitor	0.7442
	CYP450 3A4 Inhibitor	0.8150
	CYP Inhibitory Promiscuity	0.8350
Toxicity	Human Ether-a-go-go-Related Gene Inhibition	0.7468

Table 6. Lipinski's rule of himbacine predicted by SwissADME.

Lipinski's rule of 5	logP	Molecular weight	Molar refractivity	Hydrogen bond acceptor	Hydrogen bond donor
	4.4194	345.527 g/mol	107.03	3	0

3.7. Toxicity analysis

Toxic characteristics of himbacine were calculated by Protox II. The result predicted that drug candidate is active for hepatotoxicity and with a probability of 0.69 showing a moderate likelihood of affecting liver organ. While on the other hand it is inactive for nephrotoxicity, cardio toxicity, immunotoxicity, and carcinogenicity. Toxicity profile of himbacine compound is showing in Table 7.

Table 7. Toxicity Analysis of himbacine.

Classification	Target	Shorthand	Prediction	Probability
Organ toxicity	Hepatotoxicity	dili	Active	0.69
Organ toxicity	Nephrotoxicity	nephro	Inactive	0.90
Organ toxicity	Cardiotoxicity	cardio	Inactive	0.77
Toxicity end points	Carcinogenicity	carcino	Inactive	0.62
Toxicity end points	Immunotoxicity	immuno	Inactive	0.96
Toxicity end points	BBB-barrier	bbb	Inactive	1.0
Toxicity end points	Clinical toxicity	clinical	Inactive	0.56

Table 8. Binding free energy components (in kcal/mol) calculated using MM/GBSA and MM/PBSA methods for the receptor–ligand complex. The values represent average energy contributions ± standard error of the mean over the simulation frames.

Energy Component	MM/GBSA (kcal/mol)	MM/PBSA (kcal/mol)
ΔE_vdW	–38.41 ± 0.71	–38.41 ± 0.71
ΔE_electrostatic	–1.06 ± 0.41	–1.06 ± 0.41
ΔG_polar	+ 13.73 ± 0.50 (EGB)	+ 12.72 ± 0.66 (EPB)
ΔG_nonpolar	–4.68 ± 0.10	+ 19.75 ± 1.17 (ENPOLAR + EDISPER)
ΔG_gas	–39.47 ± 0.86	–39.47 ± 0.86
ΔG_solvation	+ 9.04 ± 0.43	+ 32.46 ± 1.28
ΔG_total	**–30.43 ± 0.53**	**–7.01 ± 0.91**

3.8. Density functional theory analysis

To evaluate the electronic structure and reactivity profile of Himbacine, Density Functional Theory (DFT) calculations were performed using the RB3LYP hybrid functional and the 6–31 G(d,p) basis set under ground-state singlet conditions (S = 0). Geometry optimization and electronic structure analysis were carried out in the gas phase. The 6–31 G(d,p) basis set was selected for its demonstrated reliability in modeling organic drug-like molecules, offering an optimal balance between computational efficiency and the accurate representation of electron distribution, particularly in conjugated systems and polar functional groups. The optimized molecular structure

yielded a total electronic energy of –1064.32494503 at. units (a.u.). The energy of the Highest Occupied Molecular Orbital (HOMO) was calculated as 0.20332 a.u., while the Lowest Unoccupied Molecular Orbital (LUMO) energy was 0.00494 a.u., resulting in a HOMO–LUMO energy gap of 0.20826 a.u., corresponding to approximately 5.66 eV. This moderate energy gap indicates a favorable compromise between thermodynamic stability and chemical reactivity, supporting the compound's potential to engage in biologically relevant interactions meanwhile maintaining structural integrity under physiological conditions.

The HOMO energy suggests a substantial electron-donating capability, enabling interaction with electrophilic residues in protein binding sites. In contrast, the LUMO energy reflects the molecule's ability to accept electron density from nucleophilic groups. This ambiphilic character enhances binding versatility and supports the formation of stabilizing non-covalent interactions, including hydrogen bonds, π–π stacking, and charge-transfer interactions. The calculated dipole moment of 5.6008 Debye indicates moderate polarity, which is consistent with desirable pharmacokinetic properties such as aqueous solubility, membrane permeability, and central nervous system bioavailability further substantiated by the ADMET analysis. Frontier molecular orbital distributions visualized in Fig. 5 show spatial separation of electron-rich (HOMO) and electron-deficient (LUMO) regions, primarily localized on polar and aromatic moieties. These regions overlap with key interaction sites identified in molecular docking and molecular dynamics simulations, which provides a coherent explanation for the compound's observed binding affinity and interaction stability.

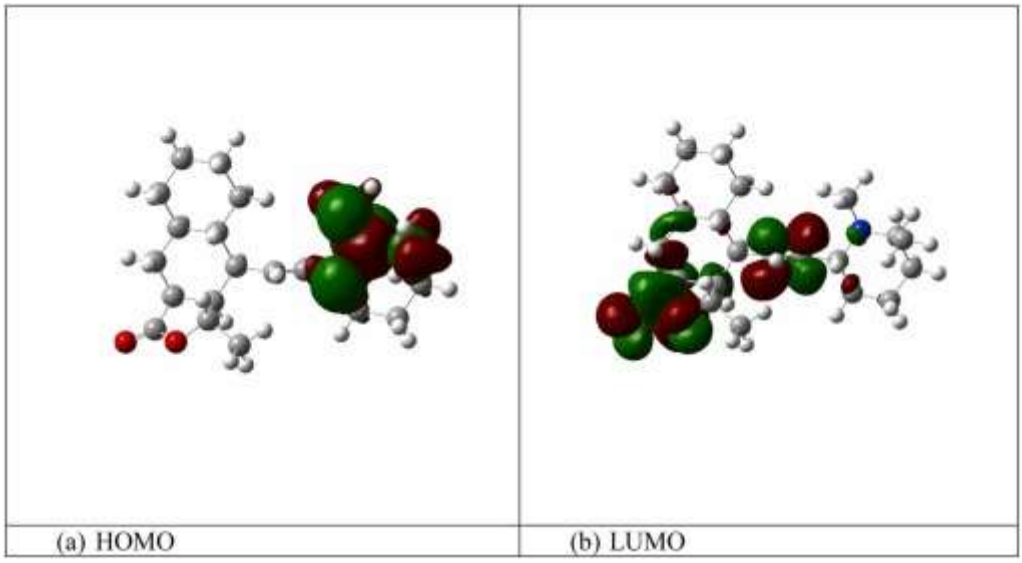

Fig. 5. Electronic distribution and potential sites for interaction, (a) Highest occupied Molecular orbital (HOMO) (b) Lowest Unoccupied Molecular orbital energy (LUMO).

Although all DFT calculations were conducted in the gas phase, this approach provides a reliable approximation of the molecule's intrinsic electronic features. Nevertheless, the absence of solvation effects constitutes a limitation, as solvent dielectric properties can modulate orbital energies and charge distribution. Incorporation of an implicit solvation model, such as the Polarizable Continuum Model (PCM), is recommended in future studies to more accurately reflect the behavior of the molecule in aqueous biological environments. Despite this, the current findings offer a robust electronic profile of Himbacine and reinforce its candidacy as a chemically stable, pharmacologically active inhibitor against *Naegleria fowleri*.

3.9. Molecular dynamic simulation

MD simulation was performed at 100 ns for hypothetical protein 4 and himbacine ligand. MD simulation was done to determine the stability of interactions among protein and ligand dock complex. MD simulations were performed using Desmond (D. E. Shaw Research). OPLS4 force field was used for all components (protein, ligand, solvent). System preparation was done using

CHARMM-GUI (free web-based tool). The protein–ligand complex was placed in an orthorhombic box with 10 Å buffer on all sides. The system was solvated with SPC water model. Na^+ and Cl^- counterions were added to neutralize the system. 0.15 M NaCl was added to mimic physiological salt concentration. Energy minimization was performed to relieve steric clashes. Equilibration involved: 100 ps NVT ensemble (300 K using Nose–Hoover thermostat). & 100 ps NPT ensemble (1 atm using Martyna–Tobias–Klein barostat). Production simulation was run for 100 ns. Time step: 2 femtoseconds. Trajectory snapshots saved every 100 ps. PME method used for electrostatics; cutoff distance: 9 Å. M-SHAKE algorithm used to constrain bonds involving hydrogen. Periodic boundary conditions applied in all directions. Molecular dynamics simulation of the himbacine–*Naegleria fowleri* protein complex revealed consistent structural stability of the ligand throughout the 100 ns trajectory. The ligand RMSD fluctuated within a narrow range (0.5–1.2 Å), indicating stable binding with no significant displacement from the active site (Fig. 6). The radius of gyration (rGyr) remained steady around 3.2–3.4 Å, suggesting that himbacine retained its compact conformation. No intramolecular hydrogen bonds were detected, implying a rigid ligand structure. Surface area analyses showed stable molecular surface area (MolSA: ~440–450 Å²), solvent-accessible surface area (SASA: ~380–420 Å²), and polar surface area (PSA: ~66–68 Å²), further confirming the ligand's conformational integrity and consistent solvent exposure. These properties collectively suggest that himbacine is a stable and well-fitting ligand for its target protein in N. fowleri. The flexibility and interaction profile of himbacine bound to *Naegleria fowleri* protein were assessed through ligand RMSF and protein–ligand contact analysis. The RMSF plot (Fig. 7) revealed moderate atomic fluctuations ranging from 3.0 to 5.3 Å, with higher mobility observed at atom indices 20–23, likely corresponding to solvent-exposed or terminal groups, while the ligand core remained stably anchored within the binding site. The protein–ligand interaction histogram (Fig. 8) demonstrated persistent and diverse contacts between himbacine and key amino acid residues. Notably, ILE 67, GLU 69, PHE 72, HIS 301, and ALA 335 exhibited strong interaction fractions, with GLU 69 and GLU 333 forming hydrogen bonds, and HIS 301 and TYR 334 participating in water-mediated interactions. The consistent hydrophobic interactions with ILE 67 and PHE 72 further supported stable ligand accommodation.

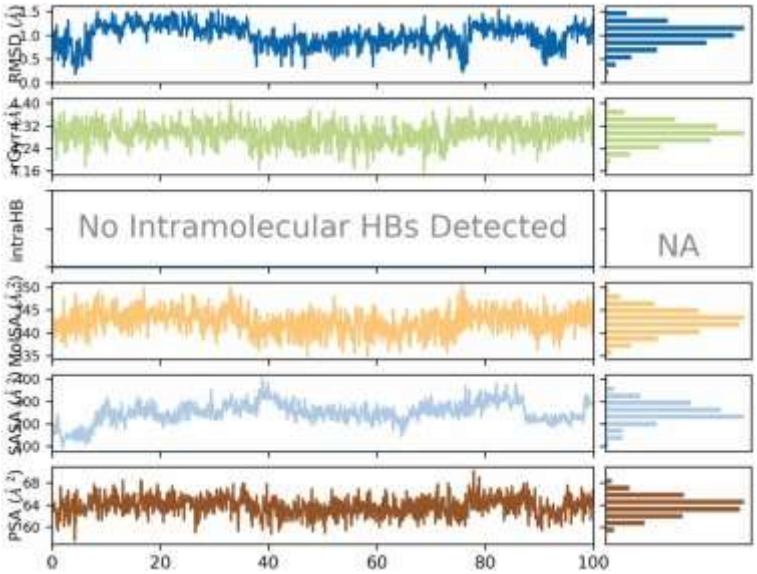

Fig. 6. Ligand property analysis of himbacine during MD simulation in complex with *Naegleria fowleri* protein.

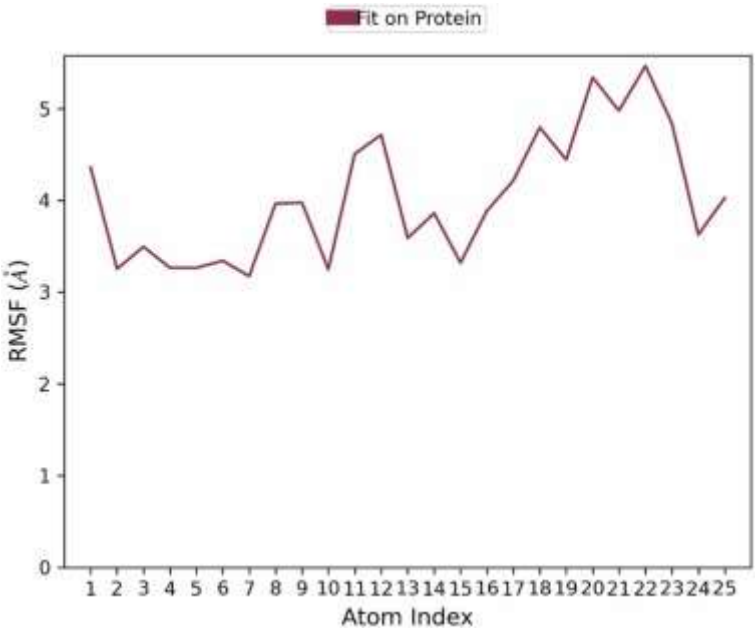

Fig. 7. Root Mean Square Fluctuation (RMSF) of ligand.

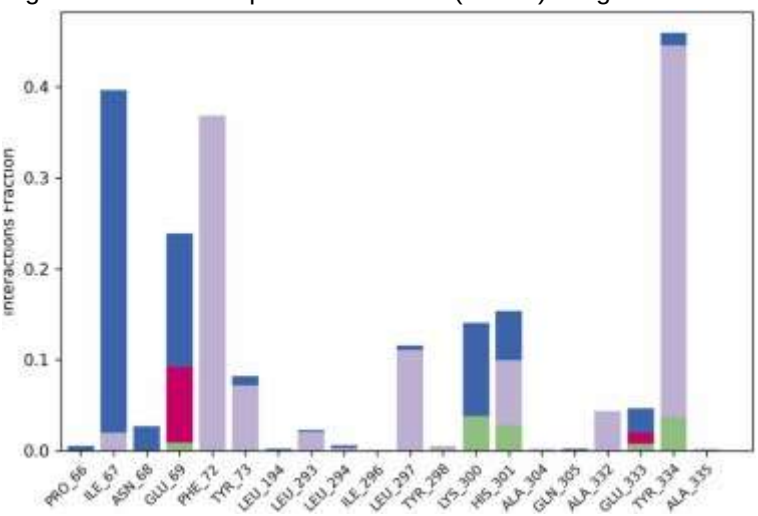

Fig. 8. Histogram of protein–ligand interactions for himbacine throughout the 100 ns MD simulation. The interaction fractions are categorized by type: hydrophobic (blue), hydrogen bonds (magenta), water bridges (green), and other interactions (violet).

The RMSD plot (Fig. 9) provides insights into the structural deviations of both the protein backbone (Cα atoms) and the ligand (himbacine) throughout the simulation. The protein RMSD stabilized around ~10.5 Å after an initial equilibration period, indicating a substantial conformational shift, potentially due to flexible or disordered regions. Conversely, the ligand RMSD, calculated by fitting on the protein, displayed fluctuations ranging between 4 Å and 9 Å, reflecting moderate positional rearrangements within the binding pocket, but suggesting that the ligand remained associated with the protein and explored different orientations without fully dissociating. The RMSF plot (Fig. 10) highlights the per-residue flexibility of the protein Cα atoms. Notably, residues at the N-terminal region exhibited the highest fluctuations (up to ~12 Å), implying intrinsic flexibility or disorder in that region. In contrast, central and C-terminal regions showed lower fluctuations, suggesting greater structural rigidity. The presence of rigid domains and flexible loops is consistent with the nature of a functionally dynamic protein, where stable domains often coordinate with more mobile regions. Fig. 11 presents the secondary structure element (SSE) timeline, which further supports the structural observations. Throughout the simulation, a consistent pattern of α-helices (depicted in red) and β-strands (in blue) was observed

across the residue indices, indicating the preservation of the overall secondary structure architecture. The upper plot of %SSE reveals that the protein maintained around 50–55 % secondary structural content throughout the simulation, suggesting no major unfolding events occurred.

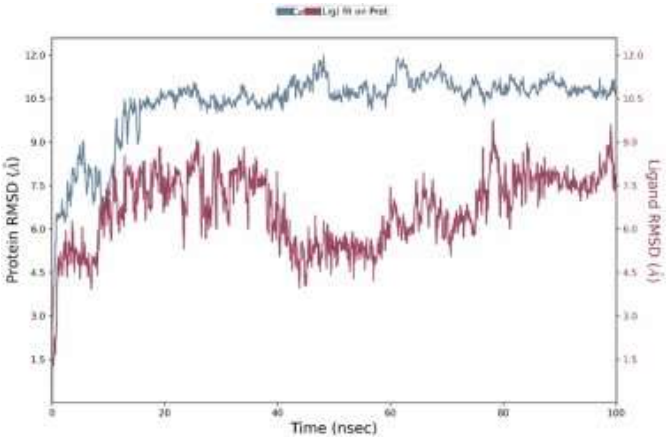

Fig. 9. Root Mean Square Deviation (RMSD) plot of the himbacine-protein complex.

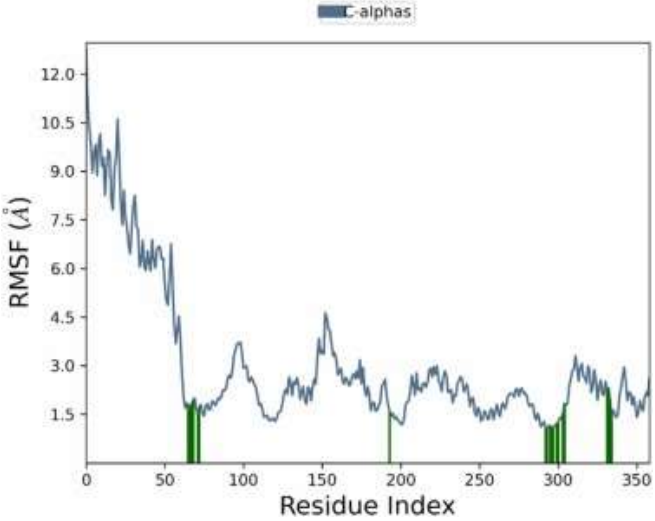

Fig. 10. Root Mean Square Fluctuation (RMSF) plot of Cα atoms for the protein.

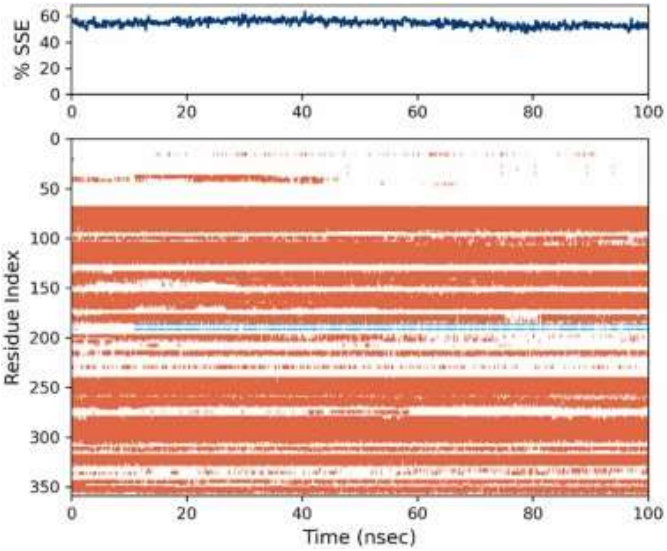

Fig. 11. Secondary Structure Element (SSE) timeline of the protein during MD simulation.

3.10. Binding free energy calculations

The binding free energy of the receptor–ligand complex was calculated using MM/GBSA and MM/PBSA methods via the MMPBSA.py module [25] in AMBER. Snapshots from the equilibrated portion of the MD trajectory were used to compute the free energies of the complex, receptor, and ligand. The binding energy was computed using the equation [26]:

Equation 1 Calculation of binding free energy (ΔG_bind) using the MM/GBSA and MM/PBSA approaches. G_complex, G_receptor, and G_ligand represent the free energies of the complex, receptor, and ligand, respectivelyΔG_bind = G_complex – (G_receptor + G_ligand)

Polar solvation energies were estimated using the Generalized Born model for MM/GBSA and the Poisson–Boltzmann model for MM/PBSA. Non-polar contributions were calculated using the solvent-accessible surface area (SASA) model [27] in MM/GBSA and the ENPOLAR/EDISPER terms in MM/PBSA. Entropic contributions were excluded from the final binding energy estimation.

4. Discussion

Naegleria fowleri, often referred to as the brain-eating amoeba, is a rare but deadly pathogen responsible for Primary Amoebic Meningoencephalitis (PAM). With a fatality rate exceeding 97 %, infections caused by this organism have drawn increasing public health concern in recent years, particularly in regions like Karachi where local outbreaks have been reported [28], [29], [30]. Although amphotericin B remains the most commonly used treatment, its efficacy is limited and often associated with toxicity. Other antibiotics like roxithromycin, zeocin, hygromycin, and clarithromycin have been explored, but no definitive or widely accepted therapy exists for this infection [31]. In light of these challenges, our study aimed to identify natural compounds with potential therapeutic effects against *N. fowleri* using a computational approach. Similar strategies have been employed in previous research, such as the in-silico screening of phytochemicals against Acanthamoeba and Trypanosoma species [32], [33], [34], [35]. However, there are very limited reports specifically targeting the Karachi strain of *N. fowleri* using computational drug discovery tools. Our approach builds on this gap by combining functional annotation, molecular docking, ADMET profiling, and molecular dynamics simulations to propose himbacine as a lead compound.

Eight toxin proteins from the *Naegleria fowleri* Karachi strain associated with diseases were obtained from the NCBI database and functionally annotated using the GO database, which predicted the function and class of proteins. Three of the eight proteins are hypothetical. Physiochemical analysis was carried out through Expasy ProtParam tool which predicted MW, instability index, theoretical isoelectric point, GRAVY, and aliphatic index of proteins. Alphafold 2 tool was employed for the prediction of proteins tertiary structure, and Molprobity tool further utilized to validate the structures, Ramachandran Plot evaluate that all protein structures were of high quality.

Virtual screening of all phytochemicals with all toxin proteins was performed using PyRx. Himbacine showed a strong binding affinity (-8.7 kcal/mol) with one of the hypothetical toxin proteins (exon 4), and the docking results were consistent with residues typically involved in protein-ligand interactions. These findings are comparable to previous studies where similar natural compounds, such as quercetin and berberine, demonstrated effective binding to microbial virulence factors [36,37]. What sets our study apart is the integration of Density Functional Theory (DFT) and MD simulation to further validate the electronic stability and dynamic behavior of the protein-ligand complex an approach not commonly seen in earlier work on *N. fowleri*.

Additionally, a preliminary sensitivity check was performed by slightly altering docking parameters (grid spacing and search space) in repeated simulations, which yielded consistent binding affinities for himbacine. This suggests a degree of robustness in the docking results, although more advanced sensitivity analyses involving ensemble docking or alternative scoring functions could be performed in future work to strengthen confidence in the ligand's predicted efficacy.MM/GBSA and MM/PBSA free energy analyses were carried out to assess the thermodynamic stability of the ligand–protein functions could be performed in future work to

strengthen confidence in the ligand's predicted efficacy. MM complexes beyond rigid docking evaluations. The calculated ΔG values revealed strong and stable interactions with the active site of the target protein, highlighting (exon 4-himbacin complex) as a promising candidate against *Naegleria fowleri*.

Overall, this study contributes to the growing field of computational drug discovery for neglected pathogens and highlights himbacine as a promising natural inhibitor with strong predicted activity, favorable ADMET profile, and stable protein-ligand interactions. These insights provide a foundation for future experimental validation and potential therapeutic development against *N. fowleri.*

5. Conclusion

The increasing number of positive cases of Primary Amoebic Meningoencephalitis caused by *Naegleria fowleri* necessitates the development of effective pharmaceuticals for prevention and treatment. Unfortunately, there are currently no approved treatments. Computer-Aided Drug design helps to identify medicinal compounds more quickly and affordably. In silico study shows that himbacine is the most effective inhibitor against *Naegleria fowleri* toxin proteins, with no toxicity and a higher binding affinity compared to other molecules. The Lipinski rule of five predicted its increased solubility and absorbance capacity, identifying it as an effective medication. The study recommends additional experimental evaluations, both in vivo and in vitro, to corroborate its findings.

Future directions and limitations

This study is only focused on computational analysis which suggests that natural inhibitors of different plants could be a promising treatment target for *Naegleria fowleri*. However, further in vitro and in vivo validations are necessary.

Declarations

None

Ethical Approval

Not applicable.

CRediT authorship contribution statement

Majid Alhomrani: Software, Data curation. **Walaa F Alsanie:** Visualization. **Abdulhakeem S Alamri:** Validation. **Tariq Aziz:** Writing – review & editing, Supervision, Resources, Project administration, Funding acquisition. **Arooj Arshad:** Methodology, Investigation, Formal analysis. **Nimra Hanif:** Writing – original draft, Methodology, Investigation. **Inmaculada Bellido Estevez:** Project administration, Data curation. **Rabia Faizan:** Methodology, Investigation, Formal analysis. **Muhammad Naveed:** Supervision, Project administration, Conceptualization.

Authors statement

All the authors agree upon submission of this manuscript to Pathology Research and Practice.

Declaration of Competing Interest

The authors declare no conflict of interest.

Acknowledgments

The authors extend their appreciation to Taif University, Saudi Arabia, for supporting this work through project number (TU-DSPP-2024–9).

Data availability

All the data generated in this research work has been included in the manuscript.

References

[1]S.K. Maciver, J.E. Piñero, J. Lorenzo-Morales. Is *naegleria fowleri* an emerging parasite?. Trends Parasitol., 36 (1) (2020), pp. 19-28

[2]M. Jahangeer, Z. Mahmood, N. Munir, U.E.A. Waraich, I.M. Tahir, M. Akram, R. Zainab. Naegleria fowleri: sources of infection, pathophysiology, diagnosis, and management; a review. Clin. Exp. Pharmacol. Physiol., 47 (2) (2020), pp. 199-212

[3]A. Alanazi, S. Younas, H. Ejaz, M. Alruwaili, Y. Alruwaili, B.B.Z. Mazhari, K. Junaid. Advancing the understanding of naegleria fowleri: global epidemiology, phylogenetic analysis, and strategies to combat a deadly pathogen. J. Infect. Public Health (2025), Article 102690

[4]V. Guerlais, N. Allouch, E.A. Moseman, A.W. Wojciechowska, J.W. Wojciechowski, I. Marceli no. Transcriptomic profiling of “brain-eating amoeba” naegleria fowleri infection in mice: the host and the protozoa perspectives. Front. Cell. Infect. Microbiol., 14 (2024), p. 1490280

[5]M. Ali, S.B. Jamal, S.M. Farhat. *naegleria fowleri* in Pakistan. Lancet Infect. Dis., 20 (1) (2020), pp. 27-28

[6]M. Barati, A.M. Chahardehi. Alkaloids: the potential of their antimicrobial activities of medicinal plants. Medicinal Plants-Chemical, Biochemical, and Pharmacological Approaches, IntechOpen (2023)

[7]P. Monika, M.N. Chandraprabha, A. Rangarajan, P.V. Waiker, K.N. Chidambara Murthy. Challenges in healing wound: role of complementary and alternative Medicine. Front. Nutr., 8 (2022), Article 791899

[8]T. Saleem, S.B. Jamal, B. Alzahrani, A. Basheer, S. Wajid Abbasi, M. Ali, M. Faheem. In-silico drug design for the novel Karachi-NF001 strain of brain-eating amoeba: naegleria fowleri. Front. Mol. Biosci., 10 (2023), p. 1098217

[9]J.-H. Kim, H.-J. Sohn, H.-J. Shin, S.E. Walz, S.-Y. Jung. Understanding the pathogenicity of naegleria fowleri in association with N. Fowleri antigen-1 (Nfa1). Parasites Hosts Dis., 62 (4) (2024), pp. 385-398

[10]H. Guan, J. Ma, Y. Sun, N.A. Khan, J. Cao, W. Yan. Genomic characterization of a novel naegleria fowleri strain isolated from karachi, Pakistan. Parasitol. Res., 120 (11) (2021), pp. 3785-3794

[11]S.H. Rangwala, A. Kuznetsov, V. Ananiev, A. Asztalos, E. Borodin, V. Evgeniev, V.A. Schne ider. Accessing NCBI data using the NCBI sequence viewer and genome data viewer (GDV). Genome Res., 31 (1) (2021), pp. 159-169

[12]S. Babichev, I. Liakh, J. Škvor. Integrating data mining, deep learning, and gene ontology analysis for gene Expression-Based disease diagnosis systems. IEEE Access (2025)

[13]M. Naveed, A. Abid, T. Aziz, A. Saleem, N. Hanif, I. Ali, A.F. Alasmari. Comparative toxicity assessment of fisetin-aided artificial intelligence-assisted drug design targeting epibulbar dermoid through phytochemicals. Open Chem., 22 (1) (2024), p. 20230197

[14]A.O. Stevens, Y. He. Benchmarking the accuracy of AlphaFold 2 in loop structure prediction. Biomolecules, 12 (7) (2022), p. 985

[15]R. Prajapat, S. Jain. Analysis the effectiveness of remdesivir, galidesivir, sofosbuvir, tenofovir and ribavirin as potential therapeutic drug target against SARS-Cov-2 RNA-Dependent RNA polymerase (RdRp): an in silico docking study. J. Res. Appl. Basic Med. Sci., 9 (3) (2023), pp. 143-153

[16]M. Naveed, N. Ain, T. Aziz, I. Ali, M. Shabbir, K. Javed, A.F. Alasmari. Revolutionizing treatment for toxic shock syndrome with engineered super chromones to combat antibiotic-resistant staphylococcus aureus. Eur. Rev. Med. Pharmacol. Sci., 27 (11) (2023)

[17]Q.Q. Lu, Y.M. Chen, H.R. Liu, J.Y. Yan, P.W. Cui, Q.F. Zhang, X.H. Gao, X. Feng, Y.Z. Liu. Nitrogen-containing flavonoid and their analogs with diverse B-ring in acetylcholinesterase and butyrylcholinesterase inhibition. Drug Dev. Res., 81 (8) (2020 Dec), pp. 1037-1047

[18]M. Naveed, N. Ali, T. Aziz, N. Hanif, M. Fatima, I. Ali, T.H. Albekairi. The natural breakthrough: phytochemicals as potent therapeutic agents against spinocerebellar ataxia type 3. Sci. Rep., 14 (1) (2024), p. 1529

[19]P. Pandey, F. Khan, K. Yadav, K. Singh, A. Rehman, A. Mazumder, M.A. Khan. Screen natural terpenoids to identify potential Jab1 inhibitors for treating breast cancer. Trends Immunother., 7 (1) (2023)
[20]E. Veg, K. Hashmi, Satya, S. Joshi, T. Khan. Computational Drug-Likeness studies of selected thiosemicarbazones: a sustainable approach for drug designing. Eng. Proc., 87 (1) (2025), p. 35
[21]B. Bakchi, A.D. Krishna, E. Sreecharan, V.B.J. Ganesh, M. Niharika, S. Maharshi, A.B. Shai k. An overview on applications of SwissADME web tool in the design and development of anticancer, antitubercular and antimicrobial agents: a medicinal chemist's perspective. J. Mol. Struct., 1259 (2022), Article 132712
[22]P. Banerjee, O.C. Ulker. Combinative ex vivo studies and in silico models ProTox-II for investigating the toxicity of chemicals used mainly in cosmetic products. Toxicol. Mech. Methods, 32 (7) (2022), pp. 542-548
[23]M. Naveed, M. Hussain, T. Aziz, N. Hanif, N. Kanwal, A. Arshad, M. Alharbi. Computational biology assisted exploration of phytochemicals derived natural inhibitors to block BZLF1 gene activation of Epstein–Bar virus in host. Sci. Rep., 14 (1) (2024), p. 31664
[24]M. Hussain, N. Kanwal, A. Jahangir, N. Ali, N. Hanif, O. Ullah. Computational modeling of cyclotides as antimicrobial agents against neisseria gonorrhoeae PorB porin protein: integration of docking, immune, and molecular dynamics simulations. Front. Chem., 12 (2024), p. 1493165
[25]B.R. Miller III, *et al.* MMPBSA. Py: an efficient program for end-state free energy calculations. J. Chem. Theory Comput., 8 (9) (2012), pp. 3314-3321
[26]S. Genheden, U. Ryde. The MM/PBSA and MM/GBSA methods to estimate ligand-binding affinities. Expert Opin. Drug Discov., 10 (5) (2015), pp. 449-461
[27]M.N. Majeed, *et al.* Designing a Multi-Epitope vaccine candidate to MERS-CoV: an in silico approach. Innov. Biosyst. Bioeng., 8 (3) (2024), pp. 3-17
[28]A. Nadeem, I.A. Malik, E.K. Afridi, F. Shariq. *naegleria fowleri* outbreak in Pakistan: unveiling the crisis and path to recovery. Front. Public Health, 11 (2023), p. 1266400
[29]I. Bodi, N. Dutt, T. Hampton, N. Akbar. Fatal granulomatous amoebic meningoencephalitis due to *balamuthia mandrillaris.* Pathol. Res Pr., 2024 (12) (2024), pp. 925-928
[30]R. Kodet, E. Nohýnková, M. Tichý, J. Soukup, G.S. Visvesvara. Amebic encephalitis caused by balamuthia mandrillaris in a Czech child: description of the first case from Europe. Pathol. Res Pr., 194 (6) (1998), pp. 423-429
[31]E. Grace, S. Asbill, K. Virga. Naegleria fowleri: pathogenesis, diagnosis, and treatment options. Antimicrob. Agents Chemother., 59 (11) (2015), pp. 6677-6681
[32]M. Naveed, K. Javed, T. Aziz, A. Abid, H.M. Rehman, M. Alharbi, A.F. Alasmari. Optimizing the resveratrol fragments for novel in silico hepatocellular carcinoma de novo drug design. Sci. Rep., 14 (1) (2024), p. 17336
[33]D.M. Baldissera, B.C. Oliveria, C.V. Rech, J.F. Rezer. Peres, M.R. Sagrillo, M.P. Alves, *et al.* Treatment with essential oil of achyrocline satureioides in rats infected with trypanosoma evansi: relationship between protective effect and tissue damage Pathol. Res Pr., 210 (12) (2014), pp. 1068-1074
[34]L.A. Eissa, A.M. Marawan, M.E. Marawan, S.A. Abass. Autophagy in disease management: exploring the potential of natural products as targeted therapies. Pathol. Res Pr., 272 (2025), Article 156077
[35]T. Khare, U. Anand, A. Dey, Y.G. Assaraf, Z.S. Chen, Z. Liu, V. Kumar. Exploring phytochemicals for combating antibiotic resistance in microbial pathogens. Front. Pharmacol., 12 (2021), Article 720726
[36]M. Naveed, I. Ali, T. Aziz, K. Javed, A. Saleem, N. Hanif, M. Alharbi. Investigating the anti-cancer compounds from calliandra harrisii for precision Medicine in pancreatic cancer via in-silico drug design and GC-MS analysis. Z. F. üR. Naturforsch. C., 79 (7-8) (2024), pp. 209-220